

Accounts

Complexes with $Fe^{III}_2(\mu\text{-O})(\mu\text{-OH})$ Core Surrounded by Hydrogen-Bonding Interaction

Yasutaka Honda, Hidekazu Arii, Takeshi Okumura, Akira Wada, Yasuhiro Funahashi, Tomohiro Ozawa, Koichiro Jitsukawa, and Hideki Masuda*

Department of Applied Chemistry, Graduate School of Engineering, Nagoya Institute of Technology, Showa-ku, Nagoya 466-8555

Received December 7, 2006; E-mail: masuda.hideki@nitech.ac.jp

Three new complexes with $Fe^{III}_2(\mu\text{-O})(\mu\text{-OH})$ core surrounded with one, two, and three amino groups, that is, (6-amino-2-pyridylmethyl)bis(pyridylmethyl)amine (MAPA), bis(6-amino-2-pyridylmethyl)(pyridylmethyl)amine (BAPA), and tris(6-amino-2-pyridylmethyl)amine (TAPA), which act as hydrogen-bonding sites, were synthesized and characterized by electronic absorption spectroscopy and X-ray diffraction analysis. Their structural bond parameters, Fe–N(pyridine), Fe–N(amine), and Fe–μ-O(H) bonds, Fe···Fe distance, and Fe–O–Fe angle, could be explained in terms of a combination of two conflicting interactions between NH_2 and μ-O(H) groups, that is, a steric repulsion and a hydrogen-bonding interactions. The LMCT bands of μ-O to iron(III) may be affected by hydrogen-bonding interactions between NH and μ-O(H) groups, which are discussed in connection with the formation processes of compound Q and compound X in sMMO and RNR-R2, respectively.

Introduction

Non-heme diiron complexes with diamond cores, such as $Fe^{III}_2(\mu\text{-O})(\mu\text{-OH})$ and $Fe^{III}_2(\mu\text{-O})_2$, have been found in soluble methane monooxygenase (sMMO),[1] ribonucleotide reductaese (RNR),[2] and fatty acid desaturases,[3] which are an important structural motif for stabilizing high oxidation states in these non-heme enzymes. The oxygenation of methane by sMMO has been proposed to occur through various intermediates, such as compound P and compound Q,[4] in which the most labile intermediate compound Q has been supposed to contain two high-spin Fe^{IV} ions based on Mössbauer spectroscopic study.[5] In model systems, although some diiron complexes, of which the ligands have consisted of carboxylate groups as an active site model in sMMO,[6–13] have been synthesized to understand the structure of compound Q, such a high valent Fe^{IV} complex has not been obtained. Recently, Que et al. have prepared of a mixed-valent $Fe^{III}Fe^{IV}(\mu\text{-O})_2$ species from the reaction of $[Fe_2(5\text{-}Et_3tpa)(\mu\text{-O})(\mu\text{-}H_3O_2)]^{3+}$ (5-Et_3tpa = tris(5-ethyl-2-pyridylmethyl)amine) with hydrogen peroxide in acetonitrile at $-40\,^{\circ}C$.[14] The donor atom set of 5-Et_3TPA the donor atoms are not carboxylate groups but N4 atoms set, and they have suggested that the structure of compound Q contains a $Fe^{IV}_2(\mu\text{-O})_2$ core. The $Fe^{III}Fe^{IV}(\mu\text{-O})_2$ species has also been generated from the O–O bond cleavage of peroxo species in the diiron–peroxo adduct $Fe^{III}_2(\mu\text{-O})(\mu\text{-O}_2)$.[15,16] The peroxo adduct compound P in the enzymatic cycle of sMMO is of importance to form compound Q. Recently, Suzuki et al. have reported that the diiron(III)–peroxo complexes with $Fe^{III}_2(\mu\text{-O})(\mu\text{-O}_2)$ and $Fe^{III}_2(\mu\text{-OH})(\mu\text{-O}_2)$ cores have been investigated using structural analysis and spectroscopic measurements.[17] The construction of high-valent $M_2(\mu\text{-O})_2$ components is important as one of the motifs to construct a homogeneous catalyst, which activates oxygen molecule to oxidize the substrates.[18–24]

In metalloproteins, hydrogen-bonding interaction sometimes occurs between an external molecule and the active site. For example, in myoglobin (Mb), which stores oxygen molecules in muscles, the distal histidine imidazole interacts to the dioxygen molecule bound to heme iron via hydrogen bonding. Watanabe et al. have also previously reported that the mutant of Mb, Mb(F43H/H64L), in which the distal histidine has been replaced by other amino acids, shows a peroxidase-like activity,[25] indicating that hydrogen-bonding interactions supports functions of metalloproteins. So, the chemical properties of peroxo complexes may be affected by the second coordination sphere, such as a hydrophobic pocket, as well as the supporting ligand.

In order to understand the contribution of the hydrogen bond to the diamond core of $Fe^{III}_2(\mu\text{-O})(\mu\text{-O(H)})$, we designed and synthesized diiron(III) complexes of tris(2-pyridylmethyl)-amine (TPA) derivatives with one, two, and three NH_2 groups at the pyridine 6-positions (Chart 1), and their structural and electronic spectroscopic characterizations are reported.

Published on the web July 11, 2007; doi:10.1246/bcsj.80.1288

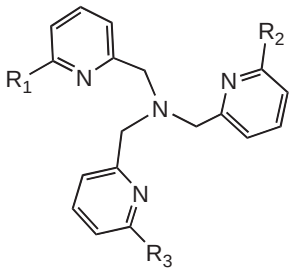

MAPA: $R_1 = NH_2$, $R_2 = R_3 = H$
BAPA: $R_1 = R_2 = NH_2$, $R_3 = H$
TAPA: $R_1 = R_2 = R_3 = NH_2$

Chart 1.

Experimental

General Procedure. All reagents used were of the highest grade available and were used without further purification. The ligands mapa[26] was synthesized according to the literature and other ligands, bapa and tapa, were prepared according to the below method. Caution: Perchlorate salts are potentially explosive and should be carefully treated!

Syntheses of Ligands, BAPA and TAPA. Bis(6-amino-2-pyridylmethyl)(2-pyridylmethyl)amine (BAPA): To an ethanol solution (500 mL) of bis(6-pivalamido-2-pyridylmethyl)(2-pyridylmethyl)amine (4.89 g, 0.01 mol) was added KOH 28.06 g (0.5 mol) dissolved to a small amount of water. The resulting solution was stirred for four days at 60 °C. The reaction products were confirmed by thin-layer chromatography ($CHCl_3$/MeOH = 7/1, $R_f = 0.05$). The solvent was evaporated under reduced pressure, and the residue was dissolved in water and extracted with CH_2Cl_2 at least five times. The CH_2Cl_2 was evaporated under reduced pressure. To a methanol solution of the residue was added active charcoal to remove an impurity. The filtrate, which was removed from the active charcoal by filtration, was evaporated to obtain a light-yellow powder. Yield: 1.60 g (50%). Calcd for BAPA·0.5H_2O ($C_{18}H_{21}N_6O_{0.5}$): C, 65.63; H, 6.43; N, 25.51%. Found: C, 65.68; H, 6.15; N, 25.81%. ^{1}H NMR (DMSO-d_6, 300 MHz): δ 3.50 (4H, s, NCH_2py), 3.73 (2H, s, NCH_2py), 5.81 (4H, s, NH_2), 6.29 (2H, d, py), 6.75 (2H, d, py), 7.24 (1H, t, py), 7.35 (2H, t, py), 7.62 (1H, d, py), 7.77 (1H, t, py), 8.48 (1H, d, py).

Tris(6-amino-2-pyridylmethyl)amine (TAPA): To an ethanol solution (500 mL) of tris(6-pivalamido-2-pyridylmethyl)amine (5.88 g, 0.01 mol) was added KOH 28.06 g (0.5 mol) dissolved in a small amount of water. The resulting solution was stirred for a week at 60 °C. The reaction product was detected by thin-layer chromatography ($CHCl_3$/MeOH = 7/1, $R_f = 0.05$). The solvent was evaporated under reduced pressure, and to the residue dissolved in methanol (20 mL) was added water (300 mL) to precipitate a white powder. The powder was collected by filtration and washed with water. The powder was recrystallized from MeOH/H_2O to obtain a light-yellow powder. Yield: 2.35 g (70%). Calcd for TAPA·0.5MeOH ($C_{18.5}H_{23}N_7O_{0.5}$): C, 63.23; H, 6.60; N, 27.90%. Found: C, 63.50; H, 6.37; N, 27.90%. ^{1}H NMR (DMSO-d_6, 90 MHz): δ 3.48 (6H, s, NCH_2py), 5.76 (6H, s, NH_2), 6.28 (3H, d, py), 6.74 (3H, d, py), 7.33 (3H, t, py).

Syntheses of Diiron(III) Complexes. $[Fe^{III}_2(mapa)_2(\mu\text{-O})(\mu\text{-OH})](ClO_4)_3$ (1a): To an acetonitrile solution (3 mL) of $Fe(ClO_4)_2$·6H_2O (72.6 mg, 0.200 mmol) was added ligand MAPA (61.0 mg, 0.200 mmol) in acetonitrile (3 mL) under an Ar atmosphere, and then the solution was exposed to air. The solvent was carefully evaporated under reduced pressure to obtain a brown powder. The powder was recrystallized over a few days from acetonitrile/diethyl ether gave red-brown crystals. Yield: 73.8 mg (70%). Calcd for **1a**·H_2O ($C_{36}H_{41}Cl_3Fe_2N_{10}O_{15}$): C, 40.34; H, 3.86; N, 13.07%. Found: C, 40.62; H, 3.70; N, 13.40%.

$[Fe^{III}_2(bapa)_2(\mu\text{-O})(\mu\text{-OH})](ClO_4)_3$ (2a): Complex **2a** was prepared by the same method as that of **1a** using BAPA in the place of MAPA. Yield: 75.9 mg (70%). Calcd for **2a** ($C_{36}H_{41}Cl_3Fe_2N_{12}O_{14}$): C, 39.89; H, 3.81; N, 15.50%. Found: C, 39.65; H, 3.76; N, 15.36%.

$[Fe^{III}_2(tapa)_2(\mu\text{-O})(\mu\text{-OH})](ClO_4)_3$ (3a): Complex **3a** was prepared by the same method as that of **1a** using TAPA in the place of MAPA. Yield: 78.0 mg (70%). Calcd for **3a** ($C_{36}H_{43}Cl_3Fe_2N_{14}O_{14}$): C, 38.81; H, 3.89; N, 17.60%. Found: C, 38.60; H, 3.91; N, 17.32%.

$[Fe^{III}_2(tapa)_2(\mu\text{-O})_2](ClO_4)_2$ (3b): To an acetonitrile solution (3 mL) of complex **3a** (55.7 mg, 0.05 mmol) was added Et_3N (5.03 mg, 0.05 mmol), of which the color changed from reddish purple to dark yellow. The solvent was evaporated under reduced pressure to obtain a reddish brown powder. Recrystallization of the powder in acetonitrile/acetone/H_2O gave single crystals. Yield: 45.2 mg (80%). Calcd for **3b**·acetone·2H_2O ($C_{38}H_{42}Cl_2Fe_2N_{14}O_{10}$·$(CH_3)_2CO$·2$H_2O$): C, 42.29; H, 4.73; N, 17.70%. Found: C, 42.38; H, 4.61; N, 17.53%.

Measurements. Electronic absorption spectra were recorded on a JASCO V-570 spectrophotometer. ^{1}H NMR spectral measurements were performed on a Varian Gemini 300 MHz or a Hitachi CR-90 NMR spectrometer in DMSO-d_6 with TMS as an internal standard. ESR spectral data were obtained on a JEOL RX-1 spectrometer at 77 K. Elemental analysis was carried out on a RECO CHN-900 corrected by acetoanilide.

X-ray Crystallography. Single crystals of **1a**, **2a**, **3a**, and **3b** suitable for X-ray diffraction analyses were obtained from methanol solutions after standing for a few days. Each crystal was mounted in a 0.7 mmϕ glass capillary, and the diffraction data were collected on a Rigaku AFC7R for **1a** and **3b** and a Rigaku RAXIS II for **2a** and **3a** using graphite monochromated Mo Kα ($\lambda = 0.71070$ Å) radiation at room temperature. Crystal data and experimental details are listed in Table 1.

All of the structures were solved by a combination of direct methods and Fourier techniques, and all of the non-hydrogen atoms were anisotropically refined by full-matrix least-squares calculations. Atomic scattering factors and anomalous dispersion terms were taken from the International Tables for X-ray Crystallography IV.[27] For all the crystals, since the numbers of reflection data were not enough to refine all the parameters of the hydrogen atoms, they were not included in further refinement; their positions were obtained from difference Fourier maps, except for some of the hydrogen atoms of water molecules. All the calculations were carried out on a Silicon Graphic workstation using the program teXsan.[28]

Crystallographic data have been deposited with Cambridge Crsyatallographic Data Centre: Deposition numbers CCDC-630397, -630398, -630399, and -630400 for compounds **1a**, **2a**, **3a**, and **3b**. Copies of the data can be obtained free of charge via http://www.ccdc.cam.ac.uk/conts/retrieving.html (or from the Cambridge Crystallographic Data Centre, 12, Union Road, Cambridge, CB2 1EZ, UK; FAX: +44 1223 336033; e-mail: deposit@ccdc.cam.ac.uk).

Results and Discussion

Preparations and Crystal Structures of 1a, 2a, 3a, and 3b. Complexes **1a**, **2a**, and **3a** were prepared according to the

Table 1. Crystal Data and Experimental Details for $[Fe^{III}_2L_2(\mu\text{-}O)(\mu\text{-}OH)](ClO_4)_3$ (L = mapa (**1a**), bapa (**2a**), and tapa (**3a**)) and $[Fe^{III}_2(tapa)_2(\mu\text{-}O)_2](ClO_4)_2$ (**3b**) Complexes

	1a·H_2O	**2a**	**3a**	**3b**·$2(CH_3)_2CO$
Formula	$C_{36}H_{41}Cl_3Fe_2N_{10}O_{15}$	$C_{36}H_{41}Cl_3Fe_2N_{12}O_{14}$	$C_{36}H_{43}Cl_3Fe_2N_{14}O_{14}$	$C_{42}H_{54}Cl_2Fe_2N_{14}O_{12}$
fw	1071.83	1083.84	1113.87	1125.54
Crystal system	Monoclinic	Monoclinic	Monoclinic	Monoclinic
Space group	$C2/c$ (#15)	$C2/c$ (#15)	$C2/c$ (#15)	$P2_1/n$ (#14)
a/Å	18.43(1)	18.846(4)	19.221(5)	11.428(3)
b/Å	10.898(7)	10.849(1)	11.178(2)	16.496(5)
c/Å	22.27(1)	22.168(2)	21.820(3)	14.075(3)
β/°	102.83(5)	104.63(1)	106.51(2)	109.30(2)
V/Å^3	4362(4)	4385(1)	4494(1)	2504(1)
Z	4	4	4	2
T/K	293	293	293	293
ρ_{calcd}/g cm^{-3}	1.632	1.641	1.646	1.493
μ(Mo Kα)/cm^{-1}	9.28	9.24	9.05	7.56
Total no. of refls.	4205	3835	3821	5478
No. of unique refls.	4058	3835	3821	5478
No. of refls. observed[a)]	1243	3386	2320	1651
No. of params	303	304	321	325
$R1/R_w$[b)]	0.063/0.068	0.072/0.117	0.090/0.144	0.065/0.083

a) $I > 3\sigma(I)$. b) $R1 = \Sigma||F_o| - |F_c||/\Sigma|F_o|$. $R_w = \{\Sigma(w(|F_o| - |F_c|)^2)/\Sigma wF_o^2\}^{1/2}$.

method described in the experimental section. Reaction of $Fe(ClO_4)_2 \cdot 6H_2O$ with tripodal ligands (L = mapa, bapa, and tapa) afforded the corresponding mononuclear iron(II) complexes $[FeL(MeCN)_2](ClO_4)_2$, and three iron(II) complexes were oxidized by exposure to O_2 in acetonitrile to afford dimer complexes **1a**, **2a**, and **3a**. Complexes **1a**, **2a**, and **3a** were obtained as reddish-purple single crystals suitable for X-ray analysis. Crystal structures, selected bond lengths and angles and intramolecular interatomic distances for **1a**, **2a**, and **3a** are shown and summarized in Fig. 1 and Table 2, respectively. The addition of 1 equiv of Et_3N to a MeCN solution containing **3a** afforded **3b**, which was also been obtained as a single crystal suitable for X-ray analysis, and its crystal structure and selected bond lengths and angles and hydrogen-bonding distances are given in Fig. 2 and Table 2, respectively.

Complexes **1a**, **2a**, and **3a** were structurally similar to each other and have a "diamond core" consisting of two Fe^{III}(mapa, bapa, or tapa) units bridged by hydroxo and oxo ligands, each of which had an inversion center located at the center of the Fe_2O_2 core. Consequently, the μ-hydroxo proton was disordered between the two oxo bridges. The presence of the proton in the formulation is supported by the presence of three perchlorate anions associated with each dinuclear unit. Each iron(III) ion had an octahedral structure coordinated with the N_4O_2 donor set, consisting of one amino and one pyridine nitrogens and two oxygens in the equatorial plane and two pyridine nitrogen atoms in the axial positions. These structures are very similar to that of $[Fe_2(6\text{-}Me_3tpa)_2(\mu\text{-}O)(\mu\text{-}OH)](ClO_4)_3$ (**4a**) reported previously.[29] The bond parameters and structures for complexes **1a**, **2a**, and **3a** were compared with those of **4a** as below (Table 3).

The average Fe–N(pyridine) bond lengths for **1a**, **2a**, and **3a** increased with an increase in the number of amino groups and are shorter than that of **4a**: **1a** (2.14 Å) < **2a** (2.16 Å) < **3a** (2.17 Å) < **4a** (2.21 Å). The Fe–N(amine) bond lengths for **1a** (2.18(1) Å), **2a** (2.172(3) Å), and **3a** (2.169(7) Å) are slightly longer than those for **4a** (2.161(7) and 2.158(11) Å). These Fe–N bond lengths lie in the range of those of the iron(III) complexes in a high-spin state,[30,31] indicating that **1a**, **2a**, and **3a** have high-spin iron(III) ions. Interestingly, the Fe–μ-O(H) bonds for **1a**, **2a**, and **3a** were distinguished by two different lengths, shorter (1.902(1), 1.899(3), and 1.911(6) Å) and longer Fe–μ-O(H) bonds (1.980(8), 2.010(3), and 2.002(7) Å), respectively, although the Fe–O bonds are likely an average between Fe–O and Fe–OH bond lengths. The respective shorter and longer bonds are trans to the amine and pyridine nitrogens of tripodal ligands. The average Fe–O bond lengths for complexes **1a**, **2a**, and **3a** were slightly longer with an increase in the number of amino groups, but they were longer than **4a**: **4a** (1.932 Å) < **1a** (1.941 Å) < **2a** (1.950 Å) < **3a** (1.956 Å). The Fe···Fe distances were also elongated with an increase in the number of amino groups (**1a** (2.839(4)) < **2a** (2.905(1)) < **3a** (2.940(2)), and the Fe–O–Fe bond angles also increased with an increase in the number of amino groups [**1a** (94.0(4)) < **2a** (95.9(1)) < **3a** (97.4(1)]. For **1a**, **2a**, and **3a**, the distances of nitrogen atom of amino groups to oxygen atom of μ-O(H) (2.96–3.10 Å), and the bond angles of N–H–O (137–154°), strongly suggested the existence of hydrogen bond between NH_2 and μ-O(H) (Table 2).

These behaviors may be explained in terms of a combination of two conflicting interactions between NH_2 and μ-O(H) groups, that is, steric repulsion and hydrogen-bonding interactions. The amino group serves not only as an electrostatically attractive interaction for μ-O(H) but also as a sterically repulsive interaction. The lengthening appeared in distances between the pyridine nitrogen atoms and iron ions can be explained by the repulsion between them. In other words, the average Fe–N(pyridine) bond lengths were elongated with an increase of the number of amino groups in the order of **1a** < **2a** < **3a** and are the longest in **4a** with three methyl groups. The lengthening in average Fe–O(H) bond lengths (**1a** < **2a** < **3a**) is attributed to the hydrogen-bonding interaction

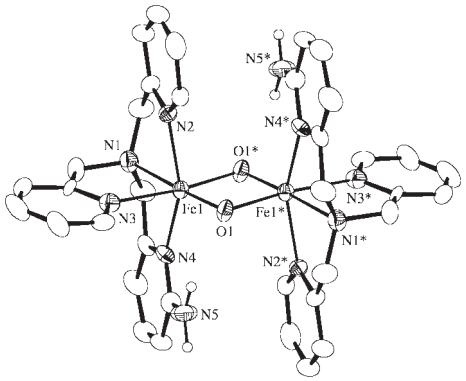

(a)

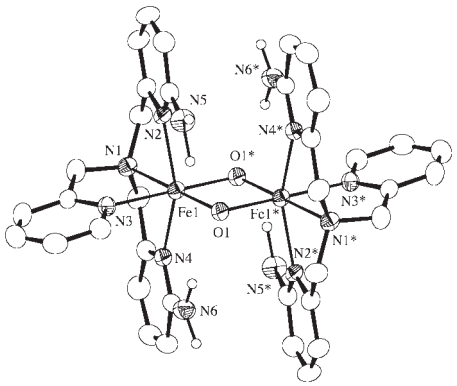

(b)

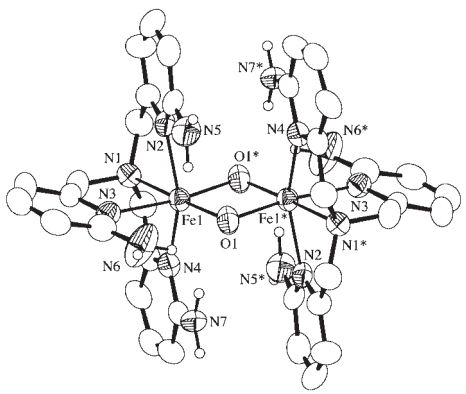

(c)

Fig. 1. ORTEP drawings of cation parts of complexes **1a** (a), **2a** (b), and **3a** (c); thermal ellipsoids are set at the 30% probability level. The atoms with and without an asterisk are related to a crystallographic inversion center each other.

Table 2. Selected Interatomic Distances and Angles for $[Fe^{III}_2L_2(\mu\text{-O})(\mu\text{-OH})](ClO_4)_3$ (L = mapa (**1a**), bapa (**2a**), and tapa (**3a**)) and $[Fe^{III}_2(tapa)_2(\mu\text{-O})_2](ClO_4)_2$ (**3b**) Complexes

	1a	**2a**	**3a**	**3b**
	Bond lengths/Å			
Fe(1)···Fe(2)	2.839(4)	2.905(1)	2.940(2)	2.706(3)
Fe(1)–O(1)	1.902(9)	1.899(3)	1.911(6)	1.874(6)
Fe(1)–O(1*)	1.980(8)	2.010(3)	2.002(7)	1.923(6)
Fe(1)–N(1)	2.18(1)	2.172(3)	2.169(7)	2.208(9)
Fe(1)–N(2)	2.15(1)	2.156(3)	2.172(7)	2.222(8)
Fe(1)–N(3)	2.17(1)	2.164(4)	2.210(8)	2.204(7)
Fe(1)–N(4)	2.11(1)	2.164(3)	2.131(7)	2.159(9)
	Bond angles/°			
Fe(1)–O(1)–Fe(1*)	94.0(4)	95.9(1)	97.4(1)	90.8(3)
O(1)–Fe(1)–O(1*)	86.0(4)	84.1(1)	82.6(3)	89.1(3)
O(1)–Fe(1)–N(1)	176.7(4)	178.4(1)	175.8(3)	177.5(3)
O(1)–Fe(1)–N(2)	99.9(4)	103.8(1)	103.1(3)	104.9(3)
O(1)–Fe(1)–N(3)	99.9(4)	101.4(1)	104.7(3)	98.4(3)
O(1)–Fe(1)–N(4)	105.5(4)	101.6(1)	101.7(3)	103.9(3)
O(1*)–Fe(1)–N(1)	94.2(4)	94.4(1)	93.3(3)	93.4(3)
O(1*)–Fe(1)–N(2)	92.2(4)	94.8(1)	91.1(3)	95.8(3)
O(1*)–Fe(1)–N(3)	173.1(5)	173.8(1)	171.7(3)	172.4(3)
O(1*)–Fe(1)–N(4)	94.9(4)	92.0(1)	94.0(3)	93.9(3)
N(1)–Fe(1)–N(2)	76.8(4)	77.0(1)	77.7(3)	75.3(3)
N(1)–Fe(1)–N(3)	79.7(5)	80.1(1)	79.5(3)	79.1(3)
N(1)–Fe(1)–N(4)	77.8(4)	77.7(1)	77.7(3)	75.6(3)
N(2)–Fe(1)–N(3)	83.3(4)	86.9(1)	83.5(3)	82.6(3)
N(2)–Fe(1)–N(4)	154.1(4)	154.2(1)	155.1(3)	149.7(3)
N(3)–Fe(1)–N(4)	87.0(4)	84.0(4)	88.4(3)	84.0(3)

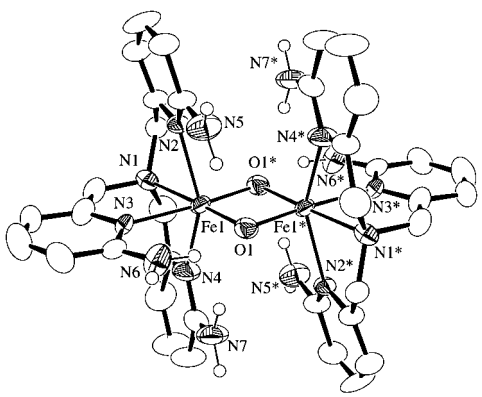

Fig. 2. ORTEP drawing of cation part of complex **3b**; thermal ellipsoids are set at the 30% probability level. The atoms with and without an asterisk are related to a crystallographic inversion center each other.

between N–H hydrogen and μ-O(H) oxygen. That is, the attractive interaction between the amino and μ-O(H) groups cause a reduction in the basicity of the μ-O(H) oxygen atoms, which decreases the coordination ability of μ-O(H) to iron(III), which results in lengthening of the Fe–μ-O(H) bonds. As a result, the lengthening in the Fe–μ-O(H) bond and increase in the Fe–O(H)–Fe angle induced a larger Fe···Fe distance: **1a** < **2a** < **3a** < **4a**.

The crystal structure of complex **3b** (Fig. 2) is essentially the same as those of complexes **1a**, **2a**, and **3a**, which is also very similar to that of $[Fe_2(6\text{-}Me_3tpa)_2(\mu\text{-O})_2](ClO_4)_2$ (**4b**) reported previously.[29] The changes in the bond parameters around the diamond cores observed between **1a**, **2a**, and **3a** and **3b** showed the same trends as seen between **4a** and **4b**: **1a**, **2a**, **3a** > **3b** (1.874(6) and 1.923(6) Å) for av. Fe–μ-O, **1a**, **2a**, **3a** > **3b** (2.706(3) Å) for Fe···Fe, **1a**, **2a**, **3a** < **3b** (2.195(9) Å) for av. Fe–N(pyridine), **1a**, **2a**, **3a** < **3b** (2.208(9) Å) for Fe–

Table 3. Comparison of Selected Interatomic Distances and Angles and λ_{max} for $[Fe^{III}_2L_2(\mu\text{-}O)(\mu\text{-}OH)](ClO_4)_3$ (L = mapa (**1a**), bapa (**2a**), tapa (**3a**), and $6Me_3$tpa (**4a**)) and $[Fe^{III}_2L_2(\mu\text{-}O)_2](ClO_4)_2$ (L = tapa (**3b**) and $6Me_3$tpa (**4b**)) Complexes

	1a	**2a**	**3a**	**3b**	**4a**[a)]	**4b**[a)]
Fe···Fe/Å	2.839(4)	2.905(1)	2.940(2)	2.948(3)	2.948(3)	2.716(2)
				2.936(3)	2.936(3)	
Fe–O/Å	1.902(9)	1.899(3)	1.911(6)	1.890(7)	1.890(7)	1.844(3)
				1.895(10)	1.895(10)	
	1.980(8)	2.010(3)	2.002(7)	1.975(7)	1.975(7)	1.916(4)
				1.968(8)	1.968(8)	
Fe–N_{am}(in-plane, N(1))/Å	2.18(1)	2.172(3)	2.169(7)	2.158(11)	2.161(7)	2.194(4)
				2.161(7)	2.158(11)	
Fe–N_{py}(in-plane, N(3))/Å	2.17(1)	2.164(4)	2.210(8)	2.204(7)	2.204(7)	2.244(4)
				2.254(9)	2.254(9)	
Fe–N_{py}(out-plane, N(2))/Å	2.15(1)	2.156(3)	2.172(7)	2.194(7)	2.194(7)	2.279(4)
				2.197(10)	2.197(10)	
Fe–N_{py}(out-plane, N(4))/Å	2.11(1)	2.164(3)	2.131(7)	2.247(7)	2.247(7)	2.255(4)
				2.179(8)	2.179(8)	
N(H)···O(H)/Å	3.10	3.042	3.07	3.04	—	—
		2.964	2.97	2.79		
			3.00	3.03		
Fe–O–Fe/deg	94.0(4)	95.9(1)	97.4(1)	90.9(3)	99.4(3)	92.5(2)
					99.2(5)	
λ_{max} (ε) in MeCN	556(1500)	520(1200)	539(1100)	620(130)	550(780)	760(80)
/nm ($M^{-1}\,cm^{-1}$)	504(1500)	470(1300)		415(320)		470(560)
	476(1500)					

a) Ref. 29.

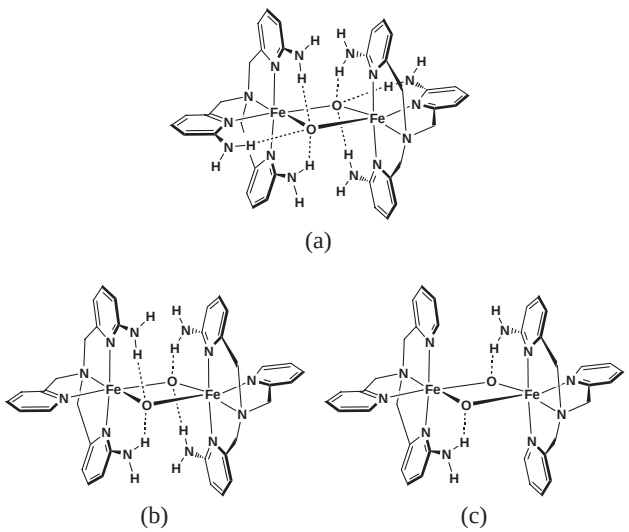

Scheme 1. Schematic views of complexes **1a**, **2a**, and **3a** showing hydrogen-bonding interaction modes.

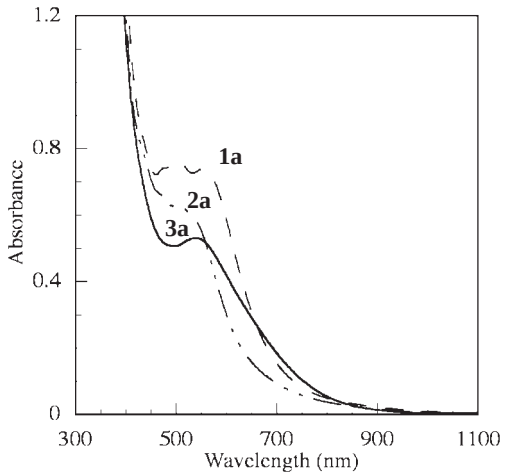

Fig. 3. Electronic absorption spectra of complexes **1a**, **2a**, and **3a** in acetonitrile solution.

N(amine), **1a**, **2a**, **3a** > **3b** (90.9(3)°) for angle Fe–O–Fe. The longer Fe–μ-O bonds and larger Fe–O–Fe angle of **3b** compared to those for **4b** (1.844(3), 1.916(4) Å and 92.5(2)°) can be explained by a electron-withdrawing effect due to hydrogen bonding (NH···μ-O = 2.79, 3,03, and 3.04 Å) (Scheme 1).

Electronic Absorption Spectra of 1a, 2a, and 3a. The electronic absorption spectra of the complexes with a diamond core $Fe_2(\mu\text{-}O)(\mu\text{-}OH)$ moiety have previously been reported to show an intense band at ca. 550 nm and weak broad band at ca. 800 nm.[29] Those of $[Fe_2(\mu\text{-}O)(\mu\text{-}OH)(tpa)_2]^{3+}$ complexes give features assignable to LMCT band of μ-oxo to iron(III) in the 600–700 nm region,[32] and those of multiply bridged (μ-oxo)diiron(III) complexes exhibit a band in the 400–530 nm region, which shifted to a lower energy region with an increase in intensity as the Fe–O–Fe angle decreases.[32] Complexes **1a**, **2a**, and **3a** studied here had characteristic LMCT bands in acetonitrile solution (Table 3 and Fig. 3), although there were no clear bands in the ≈800 nm region: 476 nm (sh, ε = 1500 $M^{-1}\,cm^{-1}$), 504 nm (ε = 1500 $M^{-1}\,cm^{-1}$), and 556 nm (ε = 1500 $M^{-1}\,cm^{-1}$) for **1a**, 470 nm (sh, ε = 1300 $M^{-1}\,cm^{-1}$) and 520 nm (ε = 1200 $M^{-1}\,cm^{-1}$) for **2a**, 539 nm (ε = 1100 $M^{-1}\,cm^{-1}$) for **3a**. The apparent red-shift in the LMCT band, as described above, was not observed as the Fe–O–Fe angles decreased, although the intensities increased in the order of

3a < **2a** < **1a**. The LMCT bands of complexes **1a** and **2a** were multiply split, and **3a**, which has the largest Fe–O–Fe angle among these three complexes, gave a single absorption band in the lowest energy region. The split bands may reflect the number of hydrogen-bonding interactions between NH_2 and μ-O(H) groups; **1a** and **2a** with one and two interaction sites, respectively, form hydrogen-bonded structures in the solution, although **3a** with three interaction sites has only one structure.

Previously, it has been reported that the addition of 1 equiv of Et_3N to acetonitrile solutions of $Fe_2(\mu\text{-O})(\mu\text{-OH})$ complexes converts them to complexes with $Fe_2(\mu\text{-O})_2$ cores, as revealed by the disappearance of the ca. ≈550 nm band and appearance of a band at ca. 470 nm band which is characteristic of the $Fe_2(\mu\text{-O})_2$ core.[29] The disappearance of the LMCT bands was also observed in our systems, but a band at ca. 470 nm was not detected because of the existence of intense bands in the region.

Biological Implication. Previously, Que et al. have reported that $[Fe_2L_2(\mu\text{-O})(\mu\text{-OH})]^{3+}$,[29] where L is tpa, tris(5-ethyl-2-pyridylmethyl)amine (5-Et$_3$tpa), *N*,*N*′-diethyl-*N*,*N*′-bis(2-pyridylmethyl)ethane-1,2-diamine (bpeen), or *N*,*N*′-dimethyl-*N*,*N*′-bis(2-pyridylmethyl)ethane-1,2-diamine (bpmen), reacted with H_2O in a large amount of water to afford to $[Fe_2L_2(\mu\text{-O})(\mu\text{-H}_3O_2)]^{3+}$. It has been interpreted that the hydration of the iron ion occurs in the case of the iron complexes with an obtuse Fe–O–Fe angle (>100°), because the obtuse Fe–O–Fe angle may make it easy for water to coordinate to iron. However, complexes **1a**, **2a**, and **3a** described here did not react with water at room temperature, which agrees with the presence of acute angles.

In the resonance Raman spectroscopic study for active mouse RNR-R2, the Fe–O–Fe symmetric vibration shifted by 5 cm^{-1} to a lower frequency upon substitution of H_2O with D_2O,[33] indicating the existence of hydrogen bonding with the μ-oxo of Fe–O–Fe. Such a hydrogen bond was not detected in sMMO. In this study, using model diiron(III) complexes with hydrogen-bonding NH_2 groups, we demonstrated that the hydrogen bond between N–H and μ-O(H) reduces the donation of μ-O(H) to iron(III), causing a longer Fe–O bond and a larger Fe···Fe separation. From the crystal structure analysis and EXAFS study on a protein and its model complexes,[34] it has been reported that both the Fe–O bond length and Fe···Fe separation in $Fe_2(\mu\text{-O})_2$ diamond core for RNR-R2 and sMMO shorten when the iron ion is in high-valent oxidation states, such as $Fe^{III}Fe^{IV}$ and $Fe^{IV}{}_2$. It has also been described that the active intermediates for RNR-R2 and sMMO are Fe^{III}–Fe^{IV} and Fe^{IV}–Fe^{IV} as compound X and compound Q, respectively, and their differences are closely related to those in their functions.[35] The results obtained here suggest that the hydrogen bond involving Fe–O–Fe detected in RNR-R2 contributes to the induction of not Fe^{IV}–Fe^{IV} but Fe^{III}–Fe^{IV} species in the active intermediate state.

This work was supported partly by a Grant-in-Aid for Scientific Research from the Ministry of Education, Culture, Sports, Science and Technology of Japan (H.M.) and supported in part by a grant from the NITECH 21st Century COE Program (H.M.), to which our thanks are due.

References

1 a) A. C. Rosenzweig, C. A. Frederick, S. J. Lippard, P. Nordlund, *Nature (London)* **1993**, *366*, 537. b) A. C. Rosenzweig, P. Nordlund, P. Takahara, C. A. Frederick, S. J. Lippard, *Chem. Biol.* **1995**, *2*, 409. c) N. Elango, R. Radhakrishnam, W. A. Froland, B. J. Wallar, C. A. Earhart, J. D. Lipscomb, D. H. Phlendorf, *Protein Sci.* **1997**, *6*, 556.

2 a) P. Nordlund, H. Eklund, *J. Mol. Biol.* **1993**, *232*, 123. b) D. T. Logan, X.-D. Su, A. Aberg, K. Regnstrom, J. Hadju, H. Eklund, P. Nordlund, *Struct. Bonding (Berlin)* **1996**, *4*, 1053.

3 Y. Lindqvist, W. Huang, G. Schneider, J. Shanklin, *EMBO J.* **1995**, *15*, 4081.

4 N. Elango, R. Radhakrishnan, W. A. Froland, B. J. Waller, C. A. Earhart, J. D. Lipscomb, D. H. Ohlendorf, *Protein Sci.* **1997**, *6*, 556.

5 K. E. Liu, A. M. Valentine, D. Wang, B. H. Huynh, D. E. Edmondson, A. Salifoglou, S. J. Lippard, *J. Am. Chem. Soc.* **1995**, *117*, 10174.

6 J. R. Hagadorn, L. Que, Jr., W. B. Tolman, *J. Am. Chem. Soc.* **1998**, *120*, 13531.

7 F. A. Chavez, R. Y. N. Ho, M. Pink, V. G. Young, Jr., S. V. Kryatov, E. V. Rybak-Akimova, H. Andres, E. Münck, L. Que, Jr., W. B. Tolman, *Angew. Chem., Int. Ed.* **2002**, *41*, 149.

8 D. Lee, B. Pierce, C. Krebs, M. P. Hendrich, B. H. Huynh, S. J. Lippard, *J. Am. Chem. Soc.* **2002**, *124*, 3993.

9 D. Lee, S. J. Lippard, *Inorg. Chem.* **2002**, *41*, 2704.

10 S. Yoon, S. J. Lippard, *J. Am. Chem. Soc.* **2005**, *127*, 8386.

11 E. C. Carson, S. J. Lippard, *Inorg. Chem.* **2006**, *45*, 828.

12 E. C. Carson, S. J. Lippard, *Inorg. Chem.* **2006**, *45*, 837.

13 K. Hashimoto, S. Nagatomo, S. Fujinami, H. Furutachi, S. Ogo, M. Suzuki, A. Uehara, Y. Maeda, Y. Watanabe, T. Kitagawa, *Angew. Chem., Int. Ed.* **2002**, *41*, 1202.

14 Y. Dong, H. Fujii, M. P. Hendrich, R. A. Leising, G. Pan, C. R. Randall, E. C. Wilkinson, Y. Zang, L. Que, Jr., B. G. Fox, K. Kauffmann, E. Münck, *J. Am. Chem. Soc.* **1995**, *117*, 2778.

15 Y. Dong, Y. Zang, L. Shu, E. C. Wilkinson, L. Que, Jr., *J. Am. Chem. Soc.* **1997**, *119*, 12683.

16 V. L. MacMurdo, H. Zheng, L. Que, Jr., *Inorg. Chem.* **2000**, *39*, 2254.

17 X. Zhang, H. Furutachi, S. Fujinami, S. Nagatomo, Y. Maeda, Y. Watanabe, T. Kitagawa, M. Suzuki, *J. Am. Chem. Soc.* **2005**, *127*, 826.

18 S. Mahapatra, J. A. Halfen, W. B. Tolman, *J. Am. Chem. Soc.* **1996**, *118*, 11575.

19 P. L. Holland, K. R. Rodgers, W. B. Tolman, *Angew. Chem., Int. Ed.* **1999**, *38*, 1139.

20 V. Mahadevan, J. L. DuBois, B. Hedman, K. O. Hodgson, T. D. P. Stack, *J. Am. Chem. Soc.* **1999**, *121*, 5583.

21 S. Itoh, M. Taki, H. Nakao, P. L. Holland, W. B. Tolman, L. Que, Jr., S. Fukuzumi, *Angew. Chem., Int. Ed.* **2000**, *39*, 398.

22 M. Taki, S. Itoh, S. Fukuzumi, *J. Am. Chem. Soc.* **2002**, *124*, 998.

23 C. X. Zhang, H.-C. Liang, E. Kim, J. Shearer, M. E. Helton, E. Kim, S. Kaderli, C. D. Incarvito, A. D. Züberbühler, A. L. Rheingold, K. Karlin, *J. Am. Chem. Soc.* **2003**, *125*, 634.

24 H. Arii, Y. Saito, S. Nagatomo, T. Kitagawa, Y. Funahashi, K. Jitsukawa, H. Masuda, *Chem. Lett.* **2003**, *32*, 156.

25 S. Ozaki, T. Matsui, Y. Watanabe, *J. Am. Chem. Soc.* **1997**, *119*, 6666.

26 S. Yamaguchi, A. Wada, Y. Funahashi, S. Nagatomo, T. Kitagawa, K. Jitsukawa, H. Masuda, *Eur. J. Inorg. Chem.* **2003**,

4378.

27 J. A. Ibers, W. C. Hamilton, in *International Tables for X-ray Crystallography Vol. IV*, Kynoch Press, Birmingham, U. K., **1974**.

28 *teXsan, Crystal Structure Analysis Package*, Molecular Structure Corporation, **1985** & **1992**.

29 H. Zheng, Y. Zang, Y. Dong, V. G. Young, Jr., L. Que, Jr., *J. Am. Chem. Soc.* **1999**, *121*, 2226.

30 Y. Zang, J. Kim, Y. Dong, E. C. Wilkinson, E. H. Appelman, L. Que, Jr., *J. Am. Chem. Soc.* **1997**, *119*, 4197.

31 H. Furutachi, Y. Ohyama, Y. Tsuchiya, K. Hashimoto, S. Fujinami, A. Uehara, M. Suzuki, Y. Maeda, *Chem. Lett.* **2000**, 1132.

32 a) S. Yan, D. D. Cox, L. L. Pearce, C. Juarez-Garcia, L. Que, Jr., J. H. Zhang, C. J. O'Connor, *Inorg. Chem.* **1989**, *28*, 2507. b) R. E. Norman, R. C. Holz, S. Menage, C. J. O'Connor, J. H. Zhang, L. Que, Jr., *Inorg. Chem.* **1990**, *29*, 4629. c) R. E. Norman, S. Yan, L. Que, Jr., G. Backes, J. Ling, J. Sanders-Loehr, J. H. Zhang, C. J. O'Connor, *J. Am. Chem. Soc.* **1990**, *112*, 1554. d) R. C. Holz, T. E. Elgren, L. L. Pearce, J. H. Zhang, C. J. O'Connor, L. Que, Jr., *Inorg. Chem.* **1993**, *32*, 5844.

33 B.-M. Sjöberg, J. Sanders-Loehr, T. M. Loehr, *Biochemistry* **1987**, *26*, 4242.

34 L. J. Shu, J. C. Nesheim, K. Kauffmann, E. Münck, J. D. Lipscomb, L. Que, Jr., *Science* **1997**, *275*, 515.

35 a) B. J. Wallar, J. D. Lipscomb, *Chem. Rev.* **1996**, *96*, 2625. b) H. Hsu, Y. Dong, L. Shu, V. G. Young, Jr., L. Que, Jr., *J. Am. Chem. Soc.* **1999**, *121*, 5230.

Yasutaka Honda is a student of the Graduate School of Engineering, Nagoya Institute of Technology and a service engineer of DELL Computer. He will receive his Ph.D. in 2007 from Nagoya Institute of Technology under the direction of Prof. Hideki Masuda. His current research interests are the theoretical sciences on biologically interested transition-metal complexes.

Hidekazu Arii is a postdoctoral research fellow of Coordination Chemistry Laboratories, Institute for Molecular Science. He is moving to Gakushu-in University in 2007. He was born in Yamaguchi in 1975. He received his Ph.D. in 2003 from Nagoya Institute of Technology under the direction of Prof. Hideki Masuda. After he joined the Knowledge Cluster Initiative at Nagoya Institute of Technology as a postdoctoral, he moved to Chuo University as an assistant professor working with Prof. Makoto Chikira in 2004. In 2006, he worked as a postdoctoral research fellow at the laboratory of Dr. Hiroyuki Kawaguchi in Institute for Molecular Science. His recent researchs focus on the bio-inorganic chemical approach on nitrogen fixation.

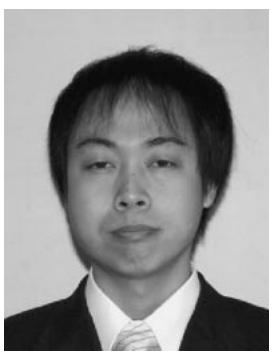

Takeshi Okumura is a student of the Graduate School of Engineering, Nagoya Institute of Technology and a member of Aichi/Nagoya Knowledge Cluster Initiative. He was born in Gifu in 1979. He received his B.S. (2003), M.S. (2005), and Ph.D. (2007) degrees from Nagoya Institute of Technology under the supervision of Professor Hideki Masuda. He will also obtain his Ph.D. in 2007 from Nagoya Institute of Technology. His current research interests include homogeneous or heterogeneous oxidation catalysts with transition-metal complexes.

Akira Wada is a researcher in Nano Medical Engineering Laboratory, Discovery Research Institute, RIKEN, 2-1 Hirosawa, Wako, Saitama 351-0198, Japan. He was a research fellow of JSPS (Japan Society for the Promotion of Science) since 1998 and received his Ph.D. from Nagoya Institute of Technology in 2001. He then moved to the Institute for Molecular Science and Tokyo Institute of Technology as a postdoctoral research fellow of JSPS. From 2004 to 2006, he researched at the National Institute of Advanced Industrial Science and Technology. In 2006, he was appointed as a research scientist at the Discovery Research Institute, RIKEN. His current research interests focus on bioinorganic chemistry, evolutionary molecular engineering, and nano biotechnology.

Tomohiro Ozawa was born in Shizuoka in 1965. He received M.S. degree in 1990 from Tsukuba University, and the Ph.D. degree in 1995 from Nagoya Institute of Technology. He was appointed as Research Assistant in 1994 at the Faculty of Engineering, Nagoya Institute of Technology and was promoted to Assistant Professor in the Graduate School of Materials Science and Technology, Nagoya Institute of Technology in 2006. His current research interests are construction of functional materials using metal–thiolate complexes with a strong ligand field.

Yasuhiro Funahashi was born in 1968 in Aichi. He received his D.Sc. degree from Nagoya University in 1999 under the supervision of Professor Osamu Yamauchi of Nagoya University. Then, he started an academic career as a research associate of Research Center for Molecular Materials, Institute for Molecular Science in Okazaki, and moved as an assistant professor to Graduate School of Engineering, Nagoya Institute of Technology in 2001. His present research focuses on syntheses of metal complexes as bio-inspired models for metalloenzymes and self-assembled molecular materials.

Koichiro Jitsukawa is a Professor of Nagoya Institute of Technology. He is moving to Osaka University in 2007. He was born in Osaka in 1953. He obtained Ph.D. degree (1983) from Osaka University under supervision of Professors Shiichiro Teranishi and Kiyotomi Kaneda. He was a JSPS fellow in 1983 and then spent eight years as a researcher at Biwako Research Laboratory of Otsuka Pharmaceutical Co., Ltd. In 1991, he moved to Nagoya Institute of Technology as an Assistant Professor. He was appointed as an Associate Professor (1995) and a Professor (2004) at Department of Materials Science and Engineering, Graduate School of Engineering, Nagoya Institute of Technology. His current research interest focuses on the design of novel multi-functional catalyst system.

Hideki Masuda is a Professor of Nagoya Institute of Technology. He was born in Kyoto in 1950. He obtained the Ph.D. degree from Kyoto University in 1982. He was appointed as a research associate at the Institute for Molecular Science in 1988, and moved to Faculty of Science, Nagoya University in 1991. He was promoted to the Graduate School of Engineering, Nagoya Institute of Technology as an associate professor in 1991 and a Professor in 1996. His current research interests include bio-inorganic chemistry, nano bio-science, and supramolecular chemistry.